SUPPORTING INFORMATION

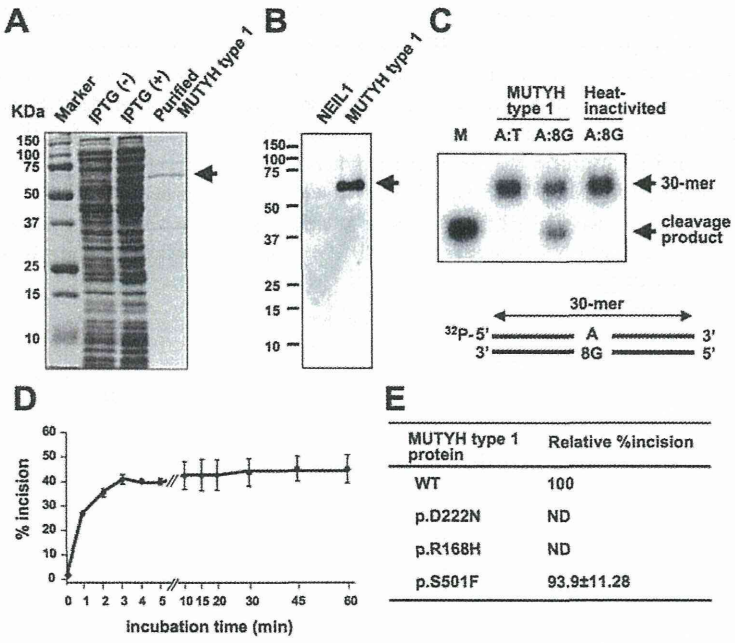

MUTYH type 1 protein	Relative %incision
WT	100
p.D222N	ND
p.R168H	ND
p.S501F	93.9±11.28

Supp. Figure S1. Measurement of DNA glycosylase activity of MUTYH type 1 protein. (**A**) Purification of wild-type MUTYH type 1 protein resolved by SDS-polyacrylamide gel electrophoresis (PAGE) and stained with Coomassie Brilliant Blue (CBB). The human MUTYH type 1 cDNA sequence was inserted into a pET25b(+) expression vector (Novagen, Darmstadt, Germany). *E. coli* BL21-CodonPlus (DE3)-RP competent cells (Stratagene, La Jolla, CA) were transformed with the MUTYH-pET25b vector and cultured at 37°C until an A_{600} of 0.6. After incubation with 0.1 mM IPTG at 20°C for 12 h, MUTYH-His_6 protein was purified with TALON metal affinity resins (Clontech, Palo Alto, CA) and a TALON 2-ml disposable gravity column (Clontech). The protein was then dialyzed against buffer containing 10 mM sodium phosphate (pH 7.6), 50 mM NaCl, 0.5 mM DTT, 0.1 mM EDTA, 0.5 mM PMSF, 2 μg/ml pepstatin, 2 μg/ml leupeptin, 50 μM chymostatin, and 10% glycerol. Lysates of *E. coli* culture without or with IPTG induction and purified MUTYH type 1 protein are shown. The arrow points to the MUTYH-His_6 protein band. (**B**) Western blot of purified wild-type MUTYH type 1 protein tagged with His_6. Purified recombinant NEIL1-His_6 protein, which was prepared by using pET25b(+) vector (Novagen) and *E. coli* BL21-CodonPlus (DE3)-RP cells (Stratagene) previously (Shinmura et al., 2004), was included as a negative control. Purified recombinant protein was mixed with an equal volume of 2x SDS sample buffer and boiled. A 2 μg protein was subjected to SDS-PAGE and electrophoretically transferred to a polyvinylidene difluoride membrane (GE Healthcare Bio-Science Corp., Piscataway, NJ). The membrane was blocked with non-fat milk and incubated with an anti-MUTYH polyclonal antibody (Ohtsubo et al., 2000). After washing, the membrane was incubated with an anti-rabbit HRP-conjugated secondary antibody (GE Healthcare Bio-Science Corp.). The membrane was then washed, and immunoreactivity was visualized with an ECL Plus chemiluminescence system (GE Healthcare Bio-Science Corp.). MUTYH-His_6 protein is indicated by the arrow. (**C**) The DNA glycosylase activity of wild-type MUTYH type 1 protein on double-stranded DNA containing an A:8-hydroxyguanine (8-OHG). 30-mer oligonucleotides containing and not containing a single 8-OHG (5'-CTG GTG GCC TGA C[8-OHG or T]C ATT CCC CAA CTA GTG-3') were chemically synthesized and purified by PAGE (Japan Bio Services, Saitama, Japan). Complementary oligonucleotides containing an adenine opposite the 8-OHG or T were ^{32}P-labeled at the 5' terminus with a MEGALABEL kit (Takara, Osaka, Japan) and a [γ-^{32}P]ATP (PerkinElmer, Tokyo, Japan), and then annealed to oligonucleotides containing a single 8-OHG or T. The reaction mixture containing 20 mM sodium phosphate (pH 7.6), 100 mM NaCl, 0.5 mM DTT, 0.5 mM EDTA, 5 μM $ZnCl_2$, 1.5% glycerol, 2.5 nM labeled oligonucleotide, 50 μg/ml BSA, and purified MUTYH protein was incubated at 37°C, and the mixture was treated with 0.1 M

NaOH at 95°C for 4 min. After adding denaturing formamide dye to the mixture, it was heated at 95°C for 3 min, and subjected to 20% PAGE. A ^{32}P-labeled marker oligonucleotide was used as a size marker for the cleavage products. The radioactivity of intact and cleaved oligonucleotides was quantified by using an FLA-3000 fluoroimage analyzer (Fuji Film, Tokyo, Japan) and ImageGauge software (Fuji Film) (Goto et al., 2009). The intact 30-mer oligonucleotides and cleavage products are indicated by the arrows. Heat-inactivation of the MUTYH protein was accomplished by heating the protein at 100°C for 5 min. 8G means 8-hydroxyguanine. (**D**) Time-course assay of cleavage of DNA containing an A:8-OHG by wild-type MUTYH type 1 protein. The MUTYH type 1 protein (260 fmole) was incubated at 37°C for 0 - 60 min with double-stranded oligonucleotide containing an A:8-OHG (50 fmole). The amount of cleavage products as a proportion of total oligonucleotides was calculated as % incision. The % incision values are shown as means ± standard errors of data from three independent experiments. (**E**) DNA glycosylase activities of wild-type MUTYH type 1 protein and their variant proteins on an A:8-OHG substrate. DNA cleavage activities of MUTYH type 1 proteins were measured at 37°C for 15 min. The amount of cleavage products as a proportion of total oligonucleotides was calculated as % incision, and the % incision of each variant-type MUTYH protein is shown relative to that of wild-type (WT) MUTYH protein, which has been set equal to 100. Values are means ± standard errors of data from three independent experiments. ND, not detected.

Detection of Lipid Peroxidation-Induced DNA Adducts Caused by 4-Oxo-2(*E*)-nonenal and 4-Oxo-2(*E*)-hexenal in Human Autopsy Tissues

Pei-Hsin Chou,[†,‡] Shinji Kageyama,[§] Shun Matsuda,[†] Keishi Kanemoto,[†] Yoshiaki Sasada,[†] Megumi Oka,[†] Kazuya Shinmura,[§] Hiroki Mori,[§] Kazuaki Kawai,[||] Hiroshi Kasai,[||] Haruhiko Sugimura,*[,§] and Tomonari Matsuda*[,†]

Research Center for Environmental Quality Management, Kyoto University, Otsu, Shiga, 520-0811, Japan, Department of Environmental Engineering, National Cheng Kung University, Tainan, 70101, Taiwan, Department of Pathology, Hamamatsu University School of Medicine, Hamamatsu, Shizuoka, 431-3192, Japan, and Department of Environmental Oncology, University of Occupational and Environmental Health, Kitakyushu, Fukuoka, 807-8555, Japan

Received February 8, 2010

DNA adducts are produced both exogenously and endogenously via exposure to various DNA-damaging agents. Two lipid peroxidation (LPO) products, 4-oxo-2(*E*)-nonenal (4-ONE) and 4-oxo-2(*E*)-hexenal (4-OHE), induce substituted etheno-DNA adducts in cells and chemically treated animals, but the adduct levels in humans have never been reported. It is important to investigate the occurrence of 4-ONE- and 4-OHE-derived DNA adducts in humans to further understand their potential impact on human health. In this study, we conducted DNA adductome analysis of several human specimens of pulmonary DNA as well as various LPO-induced DNA adducts in 68 human autopsy tissues, including colon, heart, kidney, liver, lung, pancreas, small intestine, and spleen, by liquid chromatography tandem mass spectrometry. In the adductome analysis, DNA adducts derived from 4-ONE and 4-OHE, namely, heptanone-etheno-2′-deoxycytidine (HεdC), heptanone-etheno-2′-deoxyadenosine (HεdA), and butanone-etheno-2′-deoxycytidine (BεdC), were identified as major adducts in one human pulmonary DNA. Quantitative analysis revealed 4-ONE-derived HεdC, HεdA, and heptanone-etheno-2′-deoxyguanosine (HεdG) to be ubiquitous in various human tissues at median values of 10, 15, and 8.6 adducts per 10^8 bases, respectively. More importantly, an extremely high level (more than 100 per 10^8 bases) of these DNA adducts was observed in several cases. The level of 4-OHE-derived BεdC was highly correlated with that of HεdC ($R^2 = 0.94$), although BεdC was present at about a 7-fold lower concentration than HεdC. These results suggest that 4-ONE- and 4-OHE-derived DNA adducts are likely to be significant DNA adducts in human tissues, with potential for deleterious effects on human health.

Introduction

Lipid peroxidation (LPO[1]) is a major source of DNA-damaging agents. Decomposition products generated from the LPO of polyunsaturated fatty acids (PUFAs) are highly DNA-reactive, including acrolein, crotonaldehyde, malondialdehyde, and other α,β-unsaturated aldehydes (*1–3*). These electrophilic aldehydes may modify nucleic acid bases to form DNA adducts implicated in mutagenesis, carcinogenesis, accelerated aging, or neurological deterioration (*4–6*). Thus, investigation into the levels and tissue distributions of LPO-derived DNA adducts in humans is important to further understand their possible impact on human health.

LPO-related DNA adducts identified in human tissues are mainly exocyclic etheno and propano adducts such as 1,N^6-etheno-2′-deoxyadenosine (εdA); 3,N^4-etheno-2′-deoxycytidine (εdC); 1, N^2-propano-2′-deoxyguanosines generated from acrolein, crotonaldehyde, and 4-hydroxy-2(*E*)-nonenal (4-HNE); and malondialdehyde-derived 3-(2-deoxy-β-D-erythro-pentofuranosyl)pyrimido[1,2-α]purin-10(3*H*)-one (*7–9*). The long-chain aldehyde 4-HNE is an ω-6 PUFA-peroxidation product that reacts with DNA and protein (*10–12*); furthermore, 4-HNE-related DNA adducts have been reported to be associated with carcinogenesis and Alzheimer's disease (*13–15*). 4-Oxo-2(*E*)-nonenal (4-ONE), another decomposition product of ω-6 PUFAs, has also been shown to induce the formation of etheno DNA adducts carrying aliphatic side chains both in cells and in mouse models, including heptanone-etheno-2′-deoxycytidine (HεdC), heptanone-etheno-2′-deoxyguanosine (HεdG), and heptanone-etheno-2′-deoxyadenosine (HεdA) (*16–18*). 4-Oxo-2(*E*)-hexenal (4-OHE), an ω-3 PUFA-peroxidation product having a chemical structure similar to that of 4-ONE, was recently reported to be able to produce etheno DNA adducts as well,

* Corresponding author. (H.S. (for medical questions)) E-mail: hsugimur@hama-med.ac.jp. (T.M. (for DNA adduct analysis)) E-mail: matsuda@z05.mbox.media.kyoto-u.ac.jp.

† Kyoto University.

‡ National Cheng Kung University.

§ Hamamatsu University School of Medicine.

|| University of Occupational and Environmental Health.

[1] Abbreviations: PUFA, polyunsaturated fatty acid; LPO, lipid peroxidation; 4-HNE, 4-hydroxy-2(*E*)-nonenal; 4-ONE, 4-oxo-2(*E*)-nonenal; 4-OHE, 4-oxo-2(*E*)-hexenal; HεdC, heptanone-etheno-2′-deoxycytidine; HεdG, heptanone-etheno-2′-deoxyguanosine; HεdA, heptanone-etheno-2′-deoxyadenosine; BεdC, butanone-etheno-2′-deoxycytidine; BεmedC, butanone-etheno-2′-deoxy-5-methylcytidine; BεdG, butanone-etheno-2′-deoxyguanosine; BεdA, butanone-etheno-2′-deoxyadenosine; 8-oxodG, 8-oxo-7,8-dihydro-2′-deoxyguanosine; εdA, 1,N^6-etheno-2′-deoxyadenosine; 8-OH-AdG, 8-hydroxy-1,N^2-propanodeoxyguanosine; CdG_2, α-*R*-methyl-γ-hydroxy-1,N^2-propano-2′-deoxyguanosine;COX-2, cyclooxygenase-2; HPNE, 4-hydroperoxy-2(*E*)-nonenal; EDE, 4,5-epoxy-2(*E*)-decenal; 5-LO, 5-lipoxygenase.

10.1021/tx100047d

such as butanone-etheno-2′-deoxycytidine (BεdC), butanone-etheno-2′-deoxy-5-methyl-cytidine (BεmedC), butanone-etheno-2′-deoxyguanosine (BεdG) (*19–21*), and butanone-etheno-2′-deoxyadenosine (BεdA) (*22*). The levels of 4-ONE- and 4-OHE-related DNA adducts in humans are currently unknown because such adducts were discovered only very recently.

In addition to LPO-derived DNA adducts, various other types of DNA lesions are frequently formed in humans as a consequence of exposure to environmental carcinogens or endogenous DNA-reactive agents. Because a variety of DNA adducts are present in human tissues, comprehensive investigation of these base modifications is necessary to identify the ones most critical to mutagenesis and carcinogenesis in humans. Recently, we developed a novel technique to detect multiple known or unknown DNA adducts simultaneously by using LC-MS/MS (*23, 24*). This approach, named the DNA adductome approach, monitors the neutral loss of 2′-deoxyribose from positively ionized 2′-deoxynucleoside adducts over a certain range of transitions. A variety of DNA adducts detected in DNA samples can be presented and compared by creating an adductome map showing LC retention time, mass-to-charge ratio (*m/z*), and relative peak intensity of each potential DNA adduct. In this study, we applied the DNA adductome approach to several human pulmonary DNA specimens and identified major DNA adducts on the adductome maps. Interestingly, 4-ONE- and 4-OHE-related DNA adducts were found to be major adducts in at least one pulmonary DNA sample, and they were also detected in other DNA samples. We also analyzed the levels of 4-ONE- and 4-OHE-related DNA adducts in various organs of different individuals by using LC-MS/MS. The lesions were found to be widely distributed, with some being present in significant amounts, suggesting that they could be important causative factors in human disease.

Experimental Procedures

Human Autopsy Tissues. Human autopsy tissue samples were collected at Hamamatsu University School of Medicine, Japan, and the study design was approved by the Institutional Review Board of Hamamatsu University School of Medicine (18−4). Sixty-eight samples were obtained from organs of 26 deceased persons, including the colon ($n = 6$), liver ($n = 19$), lung ($n = 12$), pancreas ($n = 9$), spleen ($n = 9$), kidney ($n = 9$), heart ($n = 2$), and small intestine ($n = 2$). The samples were taken within 24 h after death and frozen at −80 °C until DNA extraction. The ages of the subjects (17 males and 9 females) ranged from 26 to 90. Seventeen of them had malignancies as backgrounds, and final remarkable circulatory failures (shock, massive hemorrhage, and sepsis) were validated both clinically and pathologically in 6 cases. Detailed properties of the patients are listed in Supporting Information, Table S-1.

DNA Adduct Standards and Stable Isotope Standards. 4-ONE- and 4-OHE-related DNA adducts (HεdC, HεdA, HεdG, BεdC, BεmedC, BεdA, and BεdG) were synthesized according to previously published methods (*16–20*). The stereoisomers α-*S*- and α-*R*-methyl-γ-hydroxy-1,N^2-propano-2′-deoxyguanosine (CdG_1, CdG_2), 8-hydroxy-1,N^2-propanodeoxyguanosine (8-OH-AdG), and the two stereoisomers of 6-hydroxy-1,N^2-propanodeoxyguanosine (6-OH-AdG_1 and 6-OH-AdG_2) were prepared as previously described (*24*). 8-OxodG and εdA were obtained from Sigma Aldrich Japan (Japan). [U-$^{15}N_5$]-8-oxodG was kindly provided by Dr. Shinya Shibutani, State University of New York, Stony Brook, NY, [$^{15}N_5$, $^{13}C_{10}$]-2-(2′-deoxyguanosine-8-yl)-3-aminobenzanthrone ([$^{15}N_5$, $^{13}C_{10}$]-C8-C2-ABA) was kindly provided by Dr. Takeji Takamura, Kanagawa Institute of Technology, Japan, and other DNA adduct stable isotope standards were synthesized according to previously described methods using [U-$^{15}N_5$]- or [U-$^{15}N_3$]-deoxynucleosides purchased from Cambridge Isotope Laboratories (Andover, MA).

DNA Purification and Hydrolysis. Genomic DNA was isolated and purified from human autopsy samples by using a Gentra Puregene Tissue Kit (QIAGEN, Valencia, CA). DNA extraction was undertaken according to the protocol provided by the manufacturer, with the addition of desferroxamine to all solutions to a final concentration of 0.1 mM.

For DNA adductome analysis, isolated DNA was enzymatically digested as follows: each DNA sample (100 μg) was mixed with 54 μL of digestion buffer (17 mM sodium succinate and 8 mM calcium chloride, pH 6.0) containing 67.5 units of micrococcal nuclease (Worthington, Lakewood, NJ) and 0.255 units of spleen phosphodiesterase (Worthington, Lakewood, NJ). After 3 h of incubation at 37 °C, 3 units of alkaline phosphatase (Sigma-Aldrich, St. Louis, MO), 30 μL of 0.5 M Tris-HCl (pH 8.5), 15 μL of 20 mM zinc sulfate, and 101 μL of Milli-Q water were added, and the mixture were incubated for another 3 h at 37 °C. After this incubation, the mixture was concentrated to 10−20 μL by a Speed-Vac concentrator, and 100 μL of methanol was added to precipitate the protein. After centrifugation, the methanol fraction (supernatant) was transferred to a new Eppendorf tube. The precipitate was extracted with 100 μL of methanol, and the methanol fractions were combined and evaporated to dryness.

For adduct quantification analysis, the DNA sample (50 μg) was mixed with 18 μL of digestion buffer (17 mM sodium succinate and 8 mM calcium chloride, pH 6.0) containing 22.5 units of micrococcal nuclease (Worthington, Lakewood, NJ) and 0.075 units of spleen phosphodiesterase (Worthington, Lakewood, NJ) and 10 units of stable isotope-labeled DNA adduct internal standards mix, including 27.8 nM [U-$^{15}N_5$]-8-oxodG, and 1.1 nM [U-$^{15}N_5$]-εdA, [U-$^{15}N_5$]-CdG_1, [U-$^{15}N_5$]-CdG_2, [U-$^{15}N_5$]-8-OH-AdG, [U-$^{15}N_3$]-HεdC, [U-$^{15}N_5$]-HεdA, [U-$^{15}N_5$]-HεdG, [U-$^{15}N_3$]-BεdC, and [U-$^{15}N_5$]-BεdA. After 3 h of incubation at 37 °C, 3 units of alkaline phosphatase (Sigma-Aldrich, St. Louis, MO), 10 μL of 0.5 M Tris-HCl (pH 8.5), 5 μL of 20 mM zinc sulfate, and 67 μL of Milli-Q water were added, and the mixture were incubated for another 3 h at 37 °C. After this incubation, the mixture was concentrated to 10−20 μL by a Speed-Vac concentrator, and 100 μL of methanol was added to precipitate the protein. After centrifugation, the methanol fraction (supernatant) was transferred to a new Eppendorf tube. The precipitate was extracted with 100 μL of methanol, and the methanol fractions were combined and evaporated to dryness.

DNA Adductome Analysis. Digested DNA used for adductome analysis was redissolved in 120 μL of 30% dimethyl sulfoxide containing 23 nM [$^{15}N_5$, $^{13}C_{10}$]-C8-C2-ABA as the internal standard and then subjected to DNA adductome analysis similar to that described by Kanaly et al. (*24*). Briefly, adductome analysis was carried out using a Quattro Ultima Pt triple stage quadrupole mass spectrometer (Waters-Micromass, Milford, MA) equipped with a Shimadzu LC system (Shimadzu, Japan). An aliquot of digested DNA sample (10 μL) was injected and separated by a Shim-pack XR-ODS column (3.0 mm × 75 mm, Shimadzu, Japan). The column was eluted in a linear gradient of 5% to 80% methanol in water from 0 to 40 min and kept in 80% methanol in water from 40 to 45 min at a flow rate of 0.2 mL/min. Multi-reaction monitoring (MRM) was performed in positive ion mode using nitrogen as the nebulizing gas. Experimental conditions were set as follows: ion source temperature, 130 °C; desolvation temperature, 380 °C; cone voltage, 35 V; collision energy, 15 eV; desolvation gas flow rate, 700 L/h; cone gas flow rate, 35 L/h; collision gas, argon. The strategy was designed to detect the neutral loss of 2′-deoxyribose from positively ionized 2′-deoxynucleoside adducts by monitoring the samples transmitting their $[M + H]^+ \rightarrow [M + H - 116]^+$ transitions. For each DNA sample, 241 MRM transitions were monitored over the *m/z* range from transition *m/z* 250 → 134 to transition 492 → 376. For each sample injection, a total of 31 channels were monitored simultaneously with one channel for each injection reserved to monitor the internal standard [$^{15}N_5$, $^{13}C_{10}$]-C8-C2-ABA at transition *m/z* 526 → 405. Each sample was injected 8 times to complete the monitoring of 241 MRM transitions. Transitions of normal deoxynucleosides, including 252 → 136 ([dA

+ H]$^+$) and 268 → 152 ([dG + H]$^+$), were not monitored in the adductome analysis.

Relative peak intensity of each potential DNA adduct was calculated as follows: (the peak area of the potential DNA adduct)/(the peak area of the internal standard)/(the amount of 2′-deoxyguanosine (dG)). The amount of dG in each DNA sample was estimated by monitoring the dG peak area at 254 nm using the Shimazu SPD-10Avp UV−visible detector connected in series with the LC/MS/MS. The relative peak intensity was plotted as a bubble chart in which the horizontal axis was retention time and the vertical axis is *m/z*. Sodium and potassium adducts of normal deoxynucleosides or other corresponding peaks, such as those detected in the retention times of 9.3−9.5 min (dC), 10.2−10.4 min (dG), 11.2−11.4 min (dT), and 14.0−14.2 min (dA), were not included in the plot.

DNA Adduct Quantification. The digested DNA sample used for quantification was resuspended in 50 μL of 30% dimethyl sulfoxide before LC-MS/MS analysis. An aliquot (20 μL) was injected and separated by the Shim-pack XR-ODS column, eluted in a linear gradient of 5% to 30% methanol in water from 0 to 27 min, 30% to 80% from 27 to 35 min, then kept in 80% from 35 to 40 min at a flow rate of 0.2 mL/min. For the quantification of 4-ONE-derived DNA adducts, HεdC, HεdG, and HεdA, another HPLC-gradient condition was employed because of the high hydrophobicity of these compounds. A remaining aliquot (20 μL) was injected and separated by the same column, eluted in a linear gradient of 45% to 90% methanol in water from 0 to 20 min at a flow rate of 0.2 mL/min. Experimental conditions were identical to those set for adductome analysis except that the cone voltage and collision energy were different for different DNA adducts. The collision energies and characteristic reactions monitored for the different DNA adducts are as follows (cone voltage (V), collision energy (eV), base ionS → product ion): [U-$^{15}N_5$]-8-oxodG (40, 12, 288.8 → 172.8), [U-$^{15}N_5$]-εdA (35, 14, 280.9 → 164.9), [U-$^{15}N_5$]-CdG_1 and [U-$^{15}N_5$]-CdG_2 (35, 10, 343.0 → 227.0), [U-$^{15}N_5$]-8-OH-AdG (35, 10, 329.3 → 213.3), [U-$^{15}N_3$]-HεdC (35, 10, 367.0 → 251.0), [U-$^{15}N_5$]-HεdA (35, 10, 393.0 → 277.0), [U-$^{15}N_5$]-HεdG (35, 10, 409.0 → 293.0), [U-$^{15}N_3$]-BεdC (35, 10, 324.8 → 208.6), and [U-$^{15}N_5$]-BεdA (35, 10, 351.0 → 234.8), 8-oxodG (40, 12, 283.8 → 167.8), εdA (35, 14, 275.9 → 159.9), CdG_1 and CdG_2 (35, 10, 338.0 → 222.0), 8-OH-AdG, 6-OH-AdG_1, and 6-OH-AdG_2 (35, 10, 324.3 → 208.3), HεdC (35, 10, 364.0 → 248.0), HεdA (35, 10, 388.0 → 272.0), HεdG (35, 10, 404.0 → 288.0), BεdC (35, 10, 321.8 → 205.6), BεmedC (35, 20, 335.9 → 220.0), and BεdA (35, 10, 351.0 → 234.8) and BεdG (35, 20, 362.0 → 245.9).

The amount of each DNA adduct was quantified by calculating the peak area ratio of the target DNA adduct and its specific internal standard ([U-$^{15}N_3$]-BεdC was used for BεdC and BεmedC, and [U-$^{15}N_5$]-BεdA was used for BεdA and BεdG). Calibration curves were obtained by using authentic standards spiked with isotope internal standards. The concentration of dG in each DNA sample was also monitored as described in the DNA Adductome Analysis section. The number of DNA adducts per 10^8 bases was calculated by the following equation: number of DNA adducts per 10^8 bases = adduct level (fmol/μmol dG) × 0.218(μmol dG/μmol dN) × 10^{-1}, as described previously (*25*).

Results

Adductome Analysis of DNA Extracted from Human Lung Autopsy Tissues. We applied adductome analysis to DNA extracted from four human lung autopsy samples to simultaneously detect a variety of known and unknown DNA adducts in human pulmonary DNA. Although adductome analysis is semiquantitative, this analysis would help to grasp a complete picture of the DNA adducts in human samples. Several peaks were identified as corresponding to known DNA adducts by showing identical *m/z* and LC retention times to DNA adduct standards. Figure 1 shows the adductome maps of two human pulmonary DNA samples having different patterns of DNA

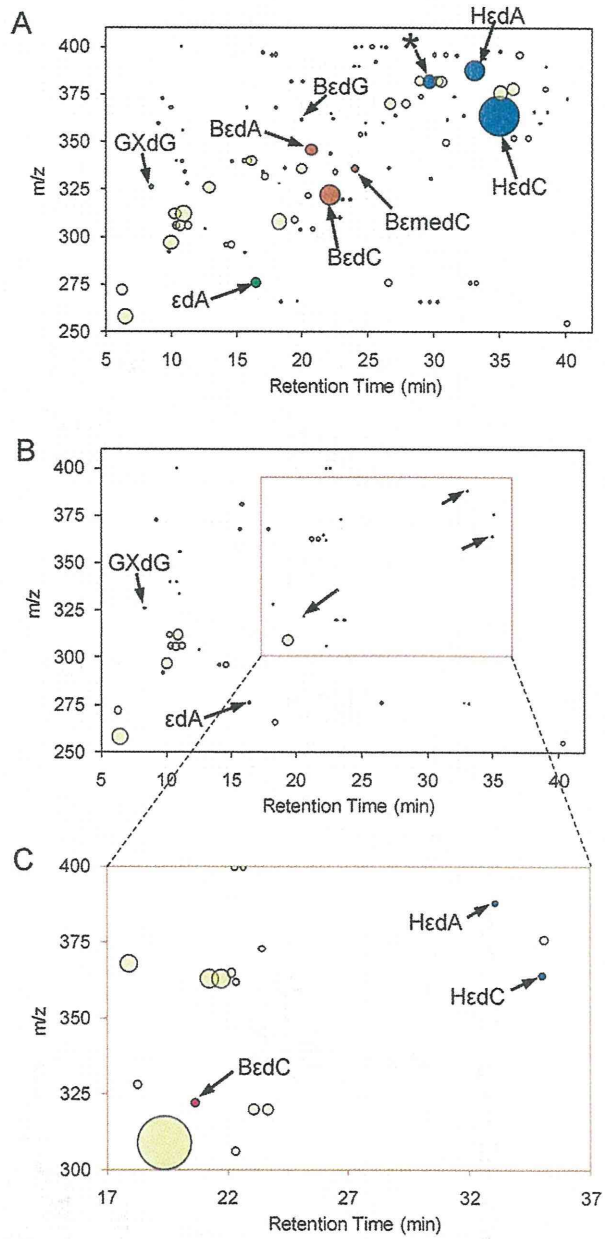

Figure 1. A and B show the DNA adductome maps of two human pulmonary DNA samples from different individuals, and C is a close-up of a selected area in B. Each circle represents one DNA adduct candidate detected by adductome analysis using LC-MS/MS. HPLC retention time, mass to charge ratio (*m/z*), and relative intensity (shown by the size of each circle, which is proportional to the peak area of each DNA adduct candidate divided by the peak area of the internal standard and the amount of 2′-deoxyguanosine) of each DNA adduct candidate can be found on the maps. Blue circles represent corresponding peaks of 4-ONE-related DNA adducts, while orange circles represent 4-OHE-related DNA adducts. Green circles are the other lipid-peroxidation derived DNA adducts, and yellow circles represent unidentified peaks. GXdG: 1,N^2-glyoxyal-dG. *: heptanone-ethano-2′-deoxycytidine.

adduct composition. Numerous DNA adducts can be seen in Figure 1A, and LPO-induced DNA adducts were detected as major peaks, including HεdC, HεdA, BεdC, BεdA, BεmedC, BεdG, εdA, and 1,N^2-glyoxal-dG. Although fewer DNA adducts were found in the sample represented in Figure 1B, LPO-induced DNA adducts derived from 4-ONE and 4-OHE (i.e., HεdC, HεdA, and BεdC) were nonetheless detected. Adductome maps of two other human pulmonary DNA samples have patterns similar to that shown in Figure 1B (data not shown),

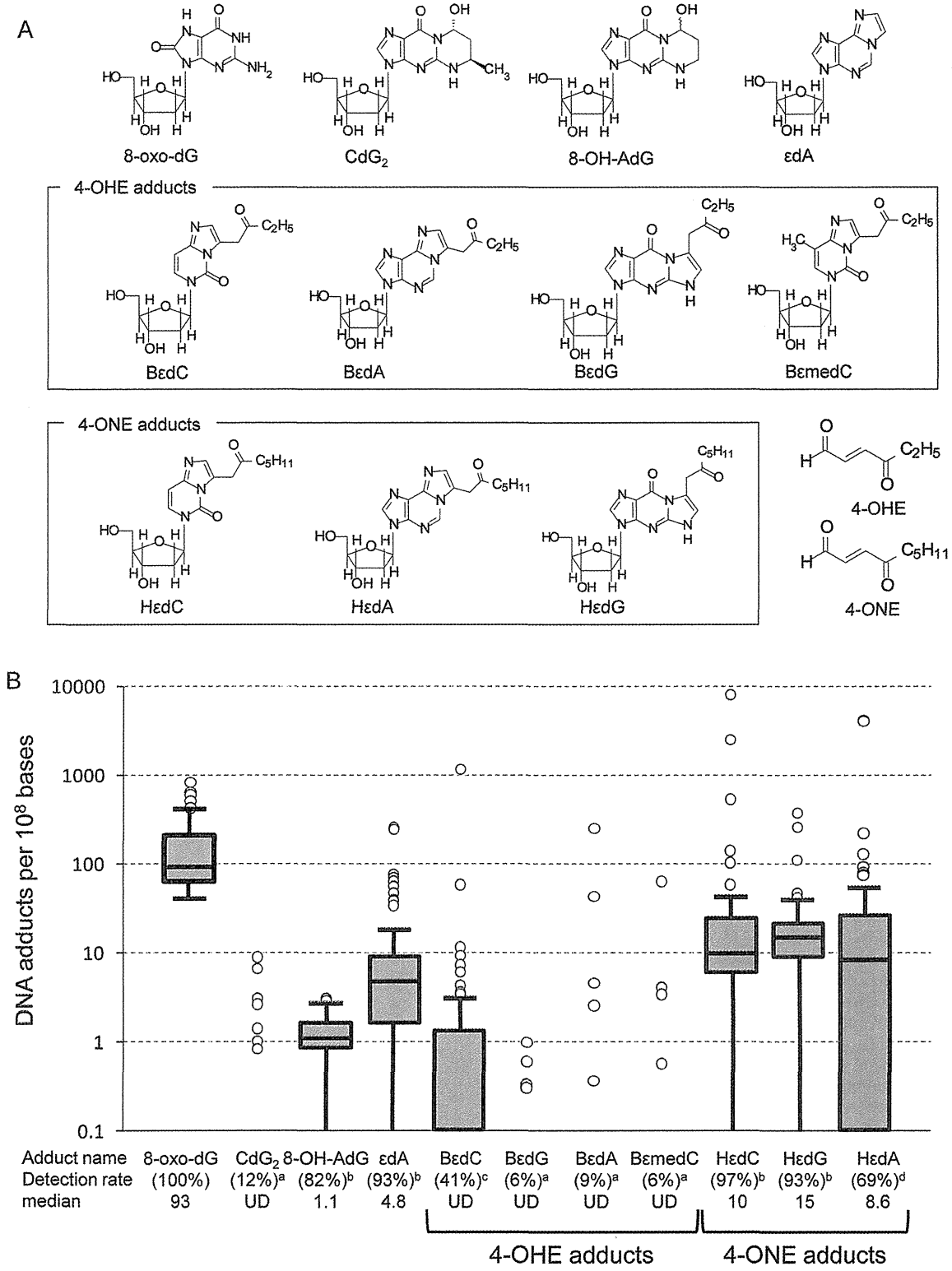

Figure 2. Level of LPO-induced DNA adducts in human tissues. (A) Chemical structure of DNA adducts detected in human tissues and the chemical structure of 4-OHE and 4-ONE. (B) Box-whisker plot of the levels of DNA adducts detected in human autopsy tissues, including the colon, liver, lung, pancreas, spleen, kidney, heart, and small intestine ($n = 68$). The boxes indicate the 75th percentile, the median, and the 25th percentile. The ends of the whiskers indicate the minimum and maximum data values unless outliers are present, in which case the whiskers extend to a maximum of 1.5 times the interquartile range. Circles above the whisker indicate outliers. Although crotonaldehyde-induced CdG_1 and acrolein-induced 6-OH-AdG_1 and 6-OH-AdG_2 were also monitored, we could not detect those adducts. Detected rate and median are shown under each DNA adduct. UD: under the detection limit. a, 75th percentile was UD; b, minimum was UD; c, median was UD; d, 25th percentile was UD.

indicating that DNA adducts induced by 4-ONE and 4-OHE are often formed in human lungs.

Detection of 4-ONE- and 4-OHE-Induced DNA Adducts in Human Autopsy Tissues. To elucidate whether the levels of

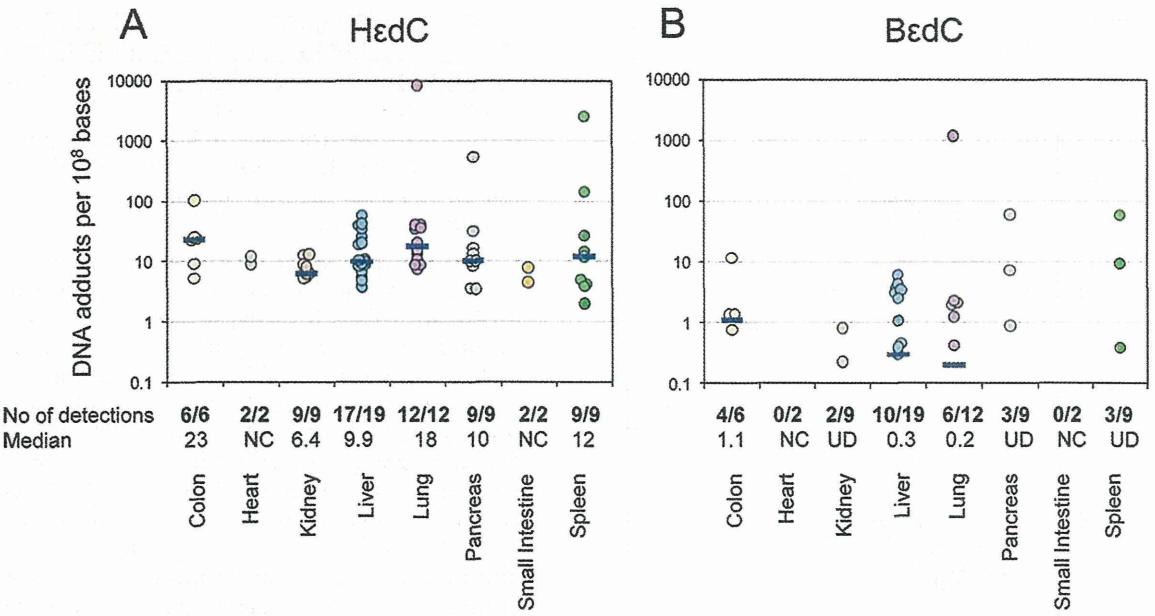

Figure 3. DNA adduct levels of HεdC and BεdC detected in various human autopsy tissues. Data from the DNA of 6 colons, 2 hearts, 9 kidneys, 19 livers, 12 lungs, 9 pancreases, 2 small intestines, and 9 spleens were plotted as circles, and the blue bars indicate the median values. NC: not calculated because the sample number was only 2. UD: median was under the detection limit.

4-ONE- and 4-OHE-related DNA adducts are comparable to those of other DNA adducts frequently found in human tissues, we measured the levels of various DNA adducts by using LC-MS/MS in 68 human autopsy specimens obtained from 26 persons, including samples of colon (n = 6), liver (n = 19), lung (n = 12), pancreas (n = 9), spleen (n = 9), kidney (n = 9), heart (n = 2), and small intestine (n = 2). The approximate detection limit of the DNA adducts (in the case that 50 μg of DNA was digested and 40% of the portion was injected to the LC/MS/MS) were as follows: 8-oxodG (1.65 adduct per 10^8 bases), εdA (0.17), CdG_1 and CdG_2 (0.17), 8-OH-AdG (0.05), 6-OH-AdG_1 and 6-OH-AdG_2 (0.08), HεdC (0.33), HεdA (1.65), HεdG (1.65), BεdC (0.17), BεmedC (0.17), and BεdA (0.83) and BεdG (0.83) (Supporting Information Figures S-2 and S-3, Table S-8), and the calibration curves of each DNA adducts are shown in Supporting Information, Figure S-4. We could detect the target DNA adducts in several human tissue samples (the representative chromatographs are shown in Supporting Information, Figures S-5, S-6, and S-7). The results revealed that the levels of target DNA adducts varied considerably among individuals or organs (Figure 2 and Supporting Information, Table S-8). Figure 2 shows the DNA adduct levels of the oxidative lesion 8-oxodG as well as the LPO-related lesions CdG_2, 8-OH-AdG, εdA, BεdC, BεdG, BεdA, BεmedC, HεdC, HεdG, and HεdA. 8-OxodG was detected in all autopsy tissues, and high detection rates were also found for εdA (93%) and 8-OH-AdG (82%). 4-ONE-related DNA adducts were also frequently detected in various tissue samples: total detection rates for HεdC, HεdG, and HεdA were 97%, 93%, and 63%, respectively. 4-OHE-related BεdC, having a total detection rate of 41%, was commonly found in the colon, liver, and lung, with detection rates higher than 50%. However, the other 4-OHE-related adducts, BεdG, BεdA, and BεmedC, showed lower detection rates of 6%, 9%, and 6%, respectively. The detection rate of the crotonaldehyde-derived DNA adduct CdG_2 was 12%. Although crotonaldehyde-induced CdG_1 and acrolein-induced 6-OH-AdG_1 and 6-OH-AdG_2 were also monitored, we could not detect those adducts in any sample. The level of each DNA adduct per 10^8 bases ranged as follows: 8-oxo-dG, 41.6−837 (median 93.2); CdG_2, not detected (ND) to 8.98 (median was under the detection limit); 8-OH-AdG, ND to 3.04 (median 1.14); εdA, ND to 259 (median 4.83); BεdC, ND to 1186 (median was under the detection limit); BεdG, ND to 0.99 (median was under the detection limit; BεdA, ND to 254 (median was under the detection limit); BεmedC, ND to 63.8 (median was under the detection limit); HεdC, ND-8204 (median 10.3); HεdG, ND to 377 (median 15.0); and HεdA, ND to 4186 (median 8.63).

Adduct Levels of HεdC and BεdC in Different Organs. As shown in Figure 3, DNA adduct levels of HεdC and BεdC range broadly in different organs. HεdC was detected in all tissue samples except for two liver specimens, whereas BεdC was detected in the colon, kidney, liver, lung, spleen, and pancreas. The median level of HεdC in different organs ranged from 6.4 (kidney) to 23 (colon) adducts per 10^8 bases, whereas the median of BεdC was 1 or 2 orders of magnitude lower. However, an extremely high level of HεdC (more than 100 adducts per 10^8 bases) was found in one colon, one lung, one pancreas and two spleen DNA samples, all from different individuals. Also, an extremely high level of BεdC was observed in one lung DNA sample, the same one that showed a high HεdC level as described above. The results suggest that 4-ONE- and 4-OHE-related DNA adducts are widely distributed in various tissues.

Figure 4 shows the correlations of BεdC, εdA, and 8-oxodG with HεdC in human tissue autopsy samples. The DNA adduct level of HεdC was strongly correlated to LPO-induced BεdC (R^2 = 0.94) and εdA (R^2 = 0.70), but no correlation could be seen between HεdC and the oxidative damage-related lesion 8-oxodG (R^2 = 0.02).

Discussion

In this study, we clearly demonstrated that DNA adducts derived from 4-ONE and 4-OHE occur commonly in human tissues. The levels of the 4-ONE-related DNA adducts HεdC, HεdA, and HεdG in human tissue samples were similar to each other (Supporting Information, Figure S-9), and their median values were 2- to 3-fold higher than that of εdA. However, the 4-OHE-related adducts BεdC, BεmedC, BεdA, and BεdG were detected at lower levels and frequencies; in most samples, their

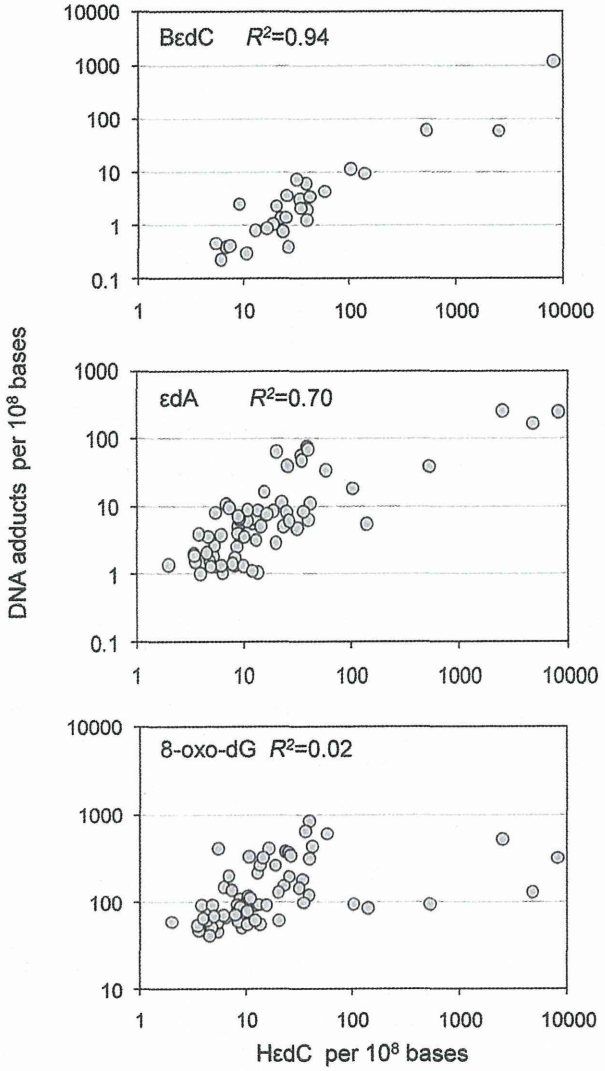

Figure 4. Correlations among DNA adduct levels of HεdC vs BεdC, εdA, and 8-oxodG. R^2: coefficient of determination. For the R^2 calculation, not detected data was treated as 0.

levels were similar to that of crotonaldehyde-derived CdG_2 or acrolein-derived 8-OH-AdG. Importantly, in some cases, the levels of these 4-ONE- and 4-OHE-derived DNA adducts were comparable to or even higher than that of the most abundant DNA adduct, 8-oxo-dG. Thus, these recently recognized DNA adducts may be an important source of somatic mutations and could significantly contribute to cancer formation in humans.

The tissues adjacent to those taken for adductome analysis were microscopically examined for the absence of tumor cells. The histological findings varied in terms of inflammation, not otherwise specified. Details of histological characteristics and their relationship to the DNA adducts level are under investigation.

Mutagenic properties of HεdC have been demonstrated in mammalian cell lines and *Escherichia coli* (*26, 27*). Pollack et al. (*26*) reported that in human cell lines HεdC blocked DNA synthesis and also miscoded markedly during the replication of a shuttle vector site-specifically modified with HεdC. The miscoding frequency was higher than 90%, and dT and dA were preferentially inserted opposite the lesion in human cells. HεdC was also shown to be genotoxic in a similar host-vector system consisting of mouse fibroblasts and a replicating plasmid bearing a site-specific HεdC (*25*). Moreover, the results indicated that the Y family DNA polymerases η, κ, and ι preferentially catalyzed the insertion of dT opposite HεdC, whereas an unidentified DNA polymerase was suggested to catalyze the insertion of dA opposite HεdC (*27*). Information about the potential mutagenic properties of the other 4-ONE- and 4-OHE-derived DNA adducts found in human autopsy tissues is still unavailable; thus, further studies concerning the mutagenicity and DNA repair pathways of these newly identified DNA adducts are necessary.

Human tissues could be exposed to 4-ONE and 4-OHE endogenously and exogenously. The endogenous formation of 4-ONE and 4-OHE is via the oxidation of ω6- and ω3-PUFAs in tissues. Because all bodily tissues contain both ω6- and ω3-PUFAs, 4-ONE and 4-OHE could be produced simultaneously under oxidative stress conditions. The near-perfect correlation between the levels of HεdC and BεdC ($R^2 = 0.94$) shown in Figure 4 strongly suggests that there is endogenous and simultaneous formation of 4-ONE- and 4-OHE-derived DNA adducts. According to the slope of the regression curve, the level of HεdC was about 7 times greater than that of BεdC. This also supports the endogenous-formation hypothesis because in all tissues except the brain, the total concentration of ω6- PUFAs is several times higher than that of ω3-PUFAs (*28, 29*).

However, no correlation was observed between the level of HεdC and the level of the oxidative DNA lesion 8-oxo-dG (Figure 4). This discrepancy may be explained by the contribution of enzymatic formation pathways to 4-ONE. For example, Blair's group demonstrated that overexpression of cyclooxygenase-2 (COX-2) increased the level of 4-ONE-derived DNA adducts in both rat intestinal epithelial cells (*30*) and the small intestine of C57BL/6J APC^{min} mice (*31*). COX-2 is an enzyme that is responsible for the formation of the important biological mediator prostaglandin H2. COX-2 can also convert arachidonic acid into 15(*S*)-hydroperoxy-5*Z*,8*Z*,11*Z*,13*E*-eicosatetraenoic acid (15-HPETE), which undergoes homolytic decomposition to the DNA-reactive bifunctional electrophiles 4-hydroperoxy-2(*E*)-nonenal (HPNE), 4,5-epoxy-2(*E*)-decenal (EDE), 4-HNE, and 4-ONE (*31*). 4-ONE is also produced enzymatically from arachidonic acid by the 5-lipoxygenase (5-LO)-related pathway (*32*). 5-LO is an enzyme that is responsible for the formation of leukotriene A_4. The precursor of leukotriene A_4, 5(*S*)-hydroperoxy-6*E*,8*Z*,11*Z*,14*Z*-eicosatetraenoic acid (5(*S*)-HPETE), generated from arachidonic acid by 5-LO, decomposes to form 4-ONE and HPNE (*32*). The considerably good correlation between the DNA adduct levels of HεdC and εdA, as described in Figure 4 ($R^2 = 0.70$), also suggests the involvement of this metabolic pathway, because εdA is known to be produced by HPNE and EDE (*31*). If 4-OHE is also produced enzymatically from abundant ω3-PUFAs such as docosahexaenoic acid, this would help to explain why the level of BεdC nearly perfectly correlates with the level of HεdC but the level of 8-oxo-dG does not. Further study is needed to elucidate this point.

The exogenous sources of 4-ONE and 4-OHE are foods and cooking vapor. Kasai and Kawai reported that several types of cooked fishes and cooking oils contain 4-OHE in the range of a few to tens of micrograms per gram (*21*). They further reported that the cooking vapor emitted during fish broiling also contains 4-OHE (*21*). In an animal experiment, orally administered 4-OHE resulted in the formation of BεdC, BεdG, and BεmedC in cells of the gastrointestinal tract, but no increase in the level of DNA adducts was observed in the liver and kidney (*19*), indicating that, except for the gastrointestinal tract, the oral route is probably not a significant source of 4-OHE. However, the

impact of cooking vapor in terms of the formation of DNA adducts in pulmonary tissues remains to be resolved.

In conclusion, DNA adducts caused by 4-ONE and 4-OHE are ubiquitous in various human tissues, and even predominant in some cases. It is very likely that these DNA adducts cause somatic mutations and cancers, contribute to aging, and have other adverse effects related to DNA damage. Further studies of their exposure routes and biological properties should be carried out to elucidate the impact of these DNA lesions on human health.

Acknowledgment. We thank H. Igarashi and T. Kamo of Hamamatsu University School of Medicine for assistance in collecting the samples. This work was supported by KAKENHI (20014007, 18181883 and 18014009); Grants-in-aid for cancer research from MHLW, Japan; the National Science Council, Taiwan (NSC 98-2221-E-006-020-MY3); NEDO, Japan; and the Smoking Research Foundation.

Supporting Information Available: Properties of the patients; sensitivity of LC/MS/MS analysis for each DNA adduct (1 and 2); calibration curves of each DNA adduct; representative chromatographs of DNA adducts, 4-OHE-derived DNA adducts, and 4-ONE-derived DNA adducts in human spleen DNA; DNA adducts level in human tissues; and correlations among the 4-ONE-derived DNA adduct level of HεdC vs HεdA (A) and HεdG (B). This material is available free of charge via the Internet at http://pubs.acs.org.

References

(1) Cajelli, E., Ferraris, A., and Brambilla, G. (1987) Mutagenicity of 4-hydroxynonenal in V79 Chinese hamster cells. *Mutat. Res. 190*, 169–171.
(2) Nath, R. G., Ocando, J. E., and Chung, F. L. (1996) Detection of 1, N2-propanodeoxyguanosine adducts as potential endogenous DNA lesions in rodent and human tissues. *Cancer Res. 56*, 452–456.
(3) Guillen, M. D., and Goicoechea, E. (2008) Toxic oxygenated alpha-,beta-unsaturated aldehydes and their study in foods: a review. *Crit. Rev. Food Sci. Nutr. 48*, 119–136.
(4) Blair, I. A. (2008) DNA adducts with lipid peroxidation products. *J. Biol. Chem. 283*, 15545–15549.
(5) Markesbery, W. R., and Carney, J. M. (1999) Oxidative alterations in Alzheimer's disease. *Brain Pathol. 9*, 133–146.
(6) Williams, M. V., Wishnok, J. S., and Tannenbaum, S. R. (2007) Covalent adducts arising from the decomposition products of lipid hydroperoxides in the presence of cytochrome c. *Chem. Res. Toxicol. 20*, 767–775.
(7) De Bont, R., and van Larebeke, N. (2004) Endogenous DNA damage in humans: a review of quantitative data. *Mutagenesis 19*, 169–185.
(8) Nair, J., De Flora, S., Izzotti, A., and Bartsch, H. (2007) Lipid peroxidation-derived etheno-DNA adducts in human atherosclerotic lesions. *Mutat. Res. 621*, 95–105.
(9) Wang, H. T., Zhang, S., Hu, Y., and Tang, M. S. (2009) Mutagenicity and Sequence Specificity of Acrolein-DNA Adducts. *Chem. Res. Toxicol. 22*, 511–517.
(10) Uchida, K. (2003) 4-Hydroxy-2-nonenal: a product and mediator of oxidative stress. *Prog. Lipid Res. 42*, 318–343.
(11) Schaur, R. J. (2003) Basic aspects of the biochemical reactivity of 4-hydroxynonenal. *Mol. Aspects Med. 24*, 149–159.
(12) Feng, Z., Hu, W., and Tang, M. S. (2004) Trans-4-hydroxy-2-nonenal inhibits nucleotide excision repair in human cells: a possible mechanism for lipid peroxidation-induced carcinogenesis. *Proc. Natl. Acad. Sci. U.S.A. 101*, 8598–8602.
(13) McGrath, L. T., McGleenon, B. M., Brennan, S., McColl, D., Mc, I. S., and Passmore, A. P. (2001) Increased oxidative stress in Alzheimer's disease as assessed with 4-hydroxynonenal but not malondialdehyde. *Q. J. Med. 94*, 485–490.
(14) Feng, Z., Hu, W., Amin, S., and Tang, M. S. (2003) Mutational spectrum and genotoxicity of the major lipid peroxidation product, trans-4-hydroxy-2-nonenal, induced DNA adducts in nucleotide excision repair-proficient and -deficient human cells. *Biochemistry 42*, 7848–7854.
(15) Zarkovic, N. (2003) 4-hydroxynonenal as a bioactive marker of pathophysiological processes. *Mol. Aspects Med. 24*, 281–291.
(16) Rindgen, D., Nakajima, M., Wehrli, S., Xu, K., and Blair, I. A. (1999) Covalent modifications to 2′-deoxyguanosine by 4-oxo-2-nonenal, a novel product of lipid peroxidation. *Chem. Res. Toxicol. 12*, 1195–1204.
(17) Rindgen, D., Lee, S. H., Nakajima, M., and Blair, I. A. (2000) Formation of a substituted 1, N(6)-etheno-2′-deoxyadenosine adduct by lipid hydroperoxide-mediated generation of 4-oxo-2-nonenal. *Chem. Res. Toxicol. 13*, 846–852.
(18) Pollack, M., Oe, T., Lee, S. H., Silva Elipe, M. V., Arison, B. H., and Blair, I. A. (2003) Characterization of 2′-deoxycytidine adducts derived from 4-oxo-2-nonenal, a novel lipid peroxidation product. *Chem. Res. Toxicol. 16*, 893–900.
(19) Kasai, H., Maekawa, M., Kawai, K., Hachisuka, K., Takahashi, Y., Nakamura, H., Sawa, R., Matsui, S., and Matsuda, T. (2005) 4-oxo-2-hexenal, a mutagen formed by omega-3 fat peroxidation, causes DNA adduct formation in mouse organs. *Ind. Health 43*, 699–701.
(20) Maekawa, M., Kawai, K., Takahashi, Y., Nakamura, H., Watanabe, T., Sawa, R., Hachisuka, K., and Kasai, H. (2006) Identification of 4-oxo-2-hexenal and other direct mutagens formed in model lipid peroxidation reactions as dGuo adducts. *Chem. Res. Toxicol. 19*, 130–138.
(21) Kasai, H., and Kawai, K. (2008) 4-oxo-2-hexenal, a mutagen formed by omega-3 fat peroxidation: occurrence, detection and adduct formation. *Mutat. Res. 659*, 56–59.
(22) Kawai, K., Chou, P. H., Matsuda, T., Inoue, M., Aaltonen, K., Savela, K., Takahashi, Y., Nakamura, H., Kimura, T., Watanabe, T., Sawa, R., Dobashi, K., Li, T. S., and Kasai, H. (2010) DNA modifications by the ω-3 lipid peroxidation-derived mutagen 4-oxo-2-hexenal in vitro and their analysis in mouse and human DNA. *Chem. Res. Toxicol. 23*, 630–636.
(23) Kanaly, R. A., Hanaoka, T., Sugimura, H., Toda, H., Matsui, S., and Matsuda, T. (2006) Development of the adductome approach to detect DNA damage in humans. *Antioxid. Redox Signaling 8*, 993–1001.
(24) Kanaly, R. A., Matsui, S., Hanaoka, T., and Matsuda, T. (2007) Application of the adductome approach to assess intertissue DNA damage variations in human lung and esophagus. *Mutat. Res. 625*, 83–93.
(25) Matsuda, T., Yabushita, H., Kanaly, R. A., Shibutani, S., and Yokoyama, A. (2006) Increased DNA damage in ALDH2-deficient alcoholics. *Chem. Res. Toxicol. 19*, 1374–1378.
(26) Pollack, M., Yang, I. Y., Kim, H. Y., Blair, I. A., and Moriya, M. (2006) Translesion DNA Synthesis across the heptanone−etheno-2′-deoxycytidine adduct in cells. *Chem. Res. Toxicol. 19*, 1074–1079.
(27) Yang, I. Y., Hashimoto, K., de Wind, N., Blair, I. A., and Moriya, M. (2009) Two distinct translesion synthesis pathways across a lipid peroxidation-derived DNA adduct in mammalian cells. *J. Biol. Chem. 284*, 191–198.
(28) Tahin, Q. S., Blum, M., and Carafoli, E. (1981) The fatty acid composition of subcellular membranes of rat liver, heart, and brain: diet-induced modifications. *Eur. J. Biochem. 121*, 5–13.
(29) Engler, M. M., Engler, M. B., Kroetz, D. L., Boswell, K. D. B., Neeley, E., and Krassner, S. M. (1999) The effects of a diet rich in docosahexaenoic acid on organ and vascular fatty acid composition in spontaneously hypertensive rats. *Prostaglandins, Leukotrienes Essent. Fatty Acids 61*, 289–295.
(30) Lee, S. H., Williams, M. V., Dubois, R. N., and Blair, I. A. (2005) Cyclooxygenase-2-mediated DNA damage. *J. Biol. Chem. 280*, 28337–28346.
(31) Williams, M. V., Lee, S. H., Pollack, M., and Blair, I. A. (2006) Endogenous lipid hydroperoxide-mediated DNA-adduct formation in min mice. *J. Biol. Chem. 281*, 10127–10133.
(32) Jian, W., Lee, S. H., Williams, M. V., and Blair, I. A. (2009) 5-Lipoxygenase-mediated endogenous DNA damage. *J. Biol. Chem. 284*, 16799–16807.

TX100047D

OPEN ACCESS Freely available online

PLoS one

SIRT1 Regulates Thyroid-Stimulating Hormone Release by Enhancing PIP5Kγ Activity through Deacetylation of Specific Lysine Residues in Mammals

Sayaka Akieda-Asai[1,2], Nobuhiro Zaima[2,3], Koji Ikegami[2,3], Tomoaki Kahyo[2,4], Ikuko Yao[2,5], Takahiro Hatanaka[2], Shun-ichiro Iemura[6], Rika Sugiyama[7], Takeaki Yokozeki[7], Yoshinobu Eishi[8], Morio Koike[8], Kyoji Ikeda[9], Takuya Chiba[10], Haruyoshi Yamaza[10,11], Isao Shimokawa[10], Si-Young Song[2], Akira Matsuno[12], Akiko Mizutani[13], Motoji Sawabe[14], Moses V. Chao[15], Masashi Tanaka[16], Yasunori Kanaho[7], Tohru Natsume[6], Haruhiko Sugimura[4], Yukari Date[1], Michael W. McBurney[17], Leonard Guarente[18], Mitsutoshi Setou[2,3]*

1 Frontier Science Research Center, University of Miyazaki, Miyazaki, Japan, **2** Mitsubishi Kagaku Institute of Life Sciences (MITILS), Tokyo, Japan, **3** Department of Molecular Anatomy, Hamamatsu University School of Medicine, Shizuoka, Japan, **4** Department of Pathology, Hamamatsu University School of Medicine, Shizuoka, Japan, **5** Department of Medical Chemistry, Kansai Medical University, Osaka, Japan, **6** National Institute of Advanced Industrial Science and Technology, Biomedicinal Information Research Center, Tokyo, Japan, **7** Department of Physiological Chemistry, Graduate School of Comprehensive Human Sciences and Institute of Basic Medical Sciences, University of Tsukuba, Ibaraki, Japan, **8** Department of Human Pathology, Tokyo Medical and Dental University, Tokyo, Japan, **9** Department of Bone and Joint Disease, Research Institute, National Center for Geriatrics and Gerontology, Aichi, Japan, **10** Department of Investigative Pathology, Nagasaki University Graduate School of Biomedical Sciences, Nagasaki, Japan, **11** Section of Pediatric Dentistry, Division of Oral Health, Growth and Development, Faculty of Dental Science, Kyushu University, Fukuoka, Japan, **12** Department of Neurosurgery, Teikyo University Chica Medical Center, Chiba, Japan, **13** Basic Medical Science and Molecular Medicine, Tokai University School of Medicine, Kanagawa, Japan, **14** Department of Pathology and Bioresource Center for Geriatric Research, Tokyo Metropolitan Geriatric Hospital and Institute of Gerontology, Tokyo, Japan, **15** Molecular Neurobiology Program, Skirball Institute of Biomolecular Medicine, New York University School of Medicine, New York, New York, United States of America, **16** Tokyo Metropolitan Institute of Gerontology, Tokyo, Japan, **17** Ottawa Hospital Research Institute and Department of Medicine, University of Ottawa, Ottawa, Canada, **18** Department of Biology, Massachusetts Institute of Technology, Cambridge, Massachusetts, United States of America

Abstract

Background: SIRT1, a NAD-dependent deacetylase, has diverse roles in a variety of organs such as regulation of endocrine function and metabolism. However, it remains to be addressed how it regulates hormone release there.

Methodology/Principal Findings: Here, we report that SIRT1 is abundantly expressed in pituitary thyrotropes and regulates thyroid hormone secretion. Manipulation of SIRT1 level revealed that SIRT1 positively regulated the exocytosis of TSH-containing granules. Using LC/MS-based interactomics, phosphatidylinositol-4-phosphate 5-kinase (PIP5K)γ was identified as a SIRT1 binding partner and deacetylation substrate. SIRT1 deacetylated two specific lysine residues (K265/K268) in PIP5Kγ and enhanced PIP5Kγ enzyme activity. SIRT1-mediated TSH secretion was abolished by PIP5Kγ knockdown. SIRT1 knockdown decreased the levels of deacetylated PIP5Kγ, $PI(4,5)P_2$, and reduced the secretion of TSH from pituitary cells. These results were also observed in SIRT1-knockout mice.

Conclusions/Significance: Our findings indicated that the control of TSH release by the SIRT1-PIP5Kγ pathway is important for regulating the metabolism of the whole body.

Citation: Akieda-Asai S, Zaima N, Ikegami K, Kahyo T, Yao I, et al. (2010) SIRT1 Regulates Thyroid-Stimulating Hormone Release by Enhancing PIP5Kγ Activity through Deacetylation of Specific Lysine Residues in Mammals. PLoS ONE 5(7): e11755. doi:10.1371/journal.pone.0011755

Editor: Mikhail V. Blagosklonny, Roswell Park Cancer Institute, United States of America

Received April 7, 2010; **Accepted** June 29, 2010; **Published** July 23, 2010

Funding: This study was supported by the Mitsubishi Kagaku Institute of Life Sciences and WAKATE S for Scientific Research to M.S. The funders had no role in study design, data collection and analysis, decision to publish, or preparation of the manuscript.

Competing Interests: The authors have declared that no competing interests exist.

* E-mail: setou@hama-med.ac.jp

Introduction

Sir2 (silent information regulator 2) is a NAD^+-dependent protein deacetylase [1,2]. In yeast, Sir2 mediates transcriptional silencing at telomeres and regulates the pace of aging [3]. In *C.elegans*, one of the Sir2 orthologues, Sir2.1, has been shown to forestall aging by acting in a *DAF-16* signaling pathway [4]. In mammals, SIRT1, the closest mammalian orthologue of Sir2, has diverse roles in a variety of organs or tissues [5], and molecular mechanisms underlying the broad SIRT1 functions are highly complicated. SIRT1 is shown to be mainly involved in the regulations of whole body metabolism and physical activity. SIRT1 promotes free fatty acid mobilization of fat from white adipose tissues by repressing peroxisome proliferator-activated receptor-γ (PPARγ), a nuclear receptor that promotes adipogenesis [6]. SIRT1 also regulates the gluconeogenic and glycolytic pathways in liver in response to fasting by interacting with and deacetylating PGC-1α, a key transcriptional regulator of glucose production [6]. SIRT1 plays other roles in stabilizing genomic DNA and proteins [7,8].

Recently, evidence has accumulated that SIRT1 could be involved in the endocrine system. In pancreas, SIRT1 modulates serum glucose levels by regulating pancreatic insulin through repressing the expression of mitochondrial uncoupling protein 2 (UCP2) [9]. In agreement with these findings, SIRT1 knockout (KO) mice show impaired glucose-stimulated insulin secretion [10]. Neuron-specific SIRT1 KO mice display reduced growth hormone level, which results in the impairment of body growth [11]. SIRT1 transgenic mice have reduced levels of blood cholesterol and adipokines, and are more metabolically active than littermate controls [12]. SIRT1 is expressed in the anorexigenic proopiomelanocortin (POMC) neurons [13], and hypothalamic SIRT1 mediates the up-regulation of the S6K pathway [14]. Despite the accumulation of evidence for the importance of SIRT1 in endocrine system, highly basic questions have remained to be addressed such as whether SIRT1 regulates metabolism in the brain and pituitary gland.

Hormones and neurotransmitters are transported as secretory granules by diverse cellular processes. Long-distance transport of these vesicles is regulated by kinesin-driven transport [15,16] and posttranslational modifications, such as tyrosination [17] and polyglutamylation [18]. When the vesicles come to the terminal points, the process is passed to the exocytotic mechanisms [19,20,21]. Phosphatidylinositol plays critical roles in this exocytotic step [22]. The phosphatidylinositol-4,5-bisphosphate ($PI(4,5)P_2$) interacts with the some proteins involved in the exocytotic machinery, such as the Ca^{2+}-dependent activator protein for secretion (CAPS) which is a priming factor, and synaptotagmin which is a Ca^{2+} sensor [23]. How SIRT1 is involved in the exocytosis machineries is poorly understood.

In the present study, we investigated how SIRT1 regulates hormone release. We identify the SIRT1 substrate, and provide evidence for a regulatory mechanism of SIRT1- and SIRT1 target-dependent hormone release.

Results

Abundant expression of SIRT1 in pituitary thyrotropes

In previous work, SIRT1 KO shows the decrease in the plasma level of thyroid hormone [24]. The report suggests that SIRT1 is involved in the regulatory axis of thyroid activity or function. We thus first investigated where SIRT1 was predominantly expressed in the whole body. To this end, we performed Western blot analyses with a commercially available anti-SIRT1 antibody on lysates obtained from a variety of adult murine tissues. These assays revealed that the expression level of the SIRT1 protein in the pituitary glands was highest among that in many other adult murine tissues (Fig. 1A). The SIRT1 expression in other tissues was detected as previous reported when the expose time was elongated (data not shown). The SIRT1 expression in the pituitary gland was also highest when compared to that in other brain tissues (Fig. 1B). We next performed immunohistochemical analysis of sagittal slices of rat brain. The immunohistochemical analysis revealed strong expression of SIRT1 in the anterior pituitary (Fig. 1C). We tested the specificity of the antibody used in Fig. 1A–C by performing Western blotting with SIRT1 KO pituitary sample as a negative control (Fig. 1D). As SIRT1 signal was not detected in the SIRT1 KO tissue sample using the antibody, the antibody has an excellent specificity (Fig. 1D).

Pituitary gland is a critical component of the endocrine system that is present in all vertebrates, and pituitary hormones control homeostasis of the whole body [25]. The anterior pituitary secretes thyroid-stimulating hormone (TSH), follicle-stimulating hormone (FSH), luteinizing hormone (LH), adrenocorticotropic hormone (ACTH), growth hormone (GH), and prolactin (PRL). We used immunohistochemistry to examine the distribution of SIRT1 among hormone-secreting pituitary cells in mice and humans. SIRT1 was most frequently localized in TSH-positive cells, but barely observable in ACTH-, FSH-, LH-, GH-, and PRL-positive cells in mice (Fig. 1E) and humans (Fig. 1F). We examined human pituitary glands that were obtained during the autopsies of 20 cadavers, ranging in age from 20 to 103 years. SIRT1-positive cells were mostly found to be localized in TSH-positive cells in the case of all the cadavers (data not shown). These results show that mammalian SIRT1 is highly abundant in thyrotropes. Although normally a nuclear protein, the SIRT1 protein was in the cytoplasm of thyrotropes (Fig. 1E and 1F), a distribution similar to that reported for alpha cells of the pancreatic islets, another type of endocrine cells [9].

SIRT1-mediated positive regulation of TSH secretion

We next examined whether SIRT1 regulates TSH secretion by manipulating SIRT1 expression level in pituitary cells. SIRT1-expression plasmids or SIRT1-RNAi was introduced by electroporation into primary cultures of rat anterior pituitary. The cultured cells expressed either increased (overexpression) or decreased (knockdown) levels of SIRT1 protein compared to the controls (Fig. 2A). SIRT1 overexpression and knockdown led to an increase and decrease, respectively, in the amount of TSH secreted into the medium (Fig. 2B).

To test the effect of SIRT1 on the release of secretory granules, we used rat pituitary cells transfected with an expression vector encoding enhanced green fluorescent protein (EGFP) fused in frame with TSHβ. TSH is a 28k-Da heterodimer composed of covalently linked α and β subunits. The α subunit is common to TSH, FSH, and LH, whereas the β subunit is specific to the TSH molecule [26]. We observed, in real-time, the motion of individual EGFP-TSHβ granules undergoing exocytosis in living cells by using total internal reflection fluorescence (TIRF) microscopy—a method that enables fluorescence excitation within a closely restricted domain situated close to the plasma membrane [21,27]. Given the characteristic of TIRF microscopy, the granule disappearance represents exocytosis of EGFP-TSHβ or returning of vesicles to cytoplasm via kiss-and-run recycling system. Thus the disappearance of granules is a result of vesicle trafficking. We recorded sequential images every 5 s (Video S1–S3) and counted the number of EGFP-positive granules that disappeared during the 5 s intervals (surrounded by red circles in Fig. 2C). The number of vanishing granules was increased in the SIRT1-overexpressing cells, and conversely decreased in the SIRT1-RNAi knockdown cells compared to the control cells (Fig. 2D). Hence, the trafficking of TSH-containing vesicles was more active in the SIRT1-overexpressing cells, and lesser in SIRT1-RNAi knockdown cells, compared to the control cells. These findings show that SIRT1 activates TSH release in thyrotropes.

Identification of PIP5Kγ as a SIRT1-binding protein

To determine the molecular mechanisms that regulate TSH release by SIRT1, we sought out the potential targets that could physically associate with SIRT1. It is known that the catalytically inactive form of protein kinase binds more avidly to its substrates than the native form of enzyme, so substrates are more effectively pulled down with the mutant enzyme compared with the wild-type